

GEOMETRIC MOTION PLANNING FOR SYSTEMS WITH TOROIDAL AND CYLINDRICAL SHAPE SPACES

Chaohui Gong
Zhongqiang Ren

Bito Robotics
Pittsburgh, Pennsylvania 15203
Email: chaohuigong@bitorobotics.com

Julian Whitman

Department of Mechanical Engineering
Carnegie Mellon University
Pittsburgh, Pennsylvania, 15213
Email: jwhitman@cmu.edu

Jaskaran Grover

Baxi Chong
Howie Choset
The Robotics Institute
Carnegie Mellon University
Pittsburgh, Pennsylvania, 15213

ABSTRACT

Kinematic motion planning using geometric mechanics tends to prescribe a trajectory in a parameterization of a shape space and determine its displacement in a position space. Often this trajectory is called a gait. Previous works assumed that the shape space is Euclidean when often it is not, either because the robotic joints can spin around forever (i.e., has an \mathbb{S}^1 configuration space component, or its parameterization has an \mathbb{S}^1 dimension). Consider a shape space that is a torus; gaits that “wrap” around the full range of a shape variable and return to its starting configuration are valid gaits in the shape space yet appear as line segments in the parameterization. Since such a gait does not form a closed loop in the parameterization, existing geometric mechanics methods cannot properly consider them. By explicitly analyzing the topology of the underlying shape space, we derive geometric tools to consider systems with toroidal and cylindrical shape spaces.

1 INTRODUCTION

Geometric mechanics has been used for gait synthesis and analysis for a variety of locomoting systems, including abstract models [1], limbless robots [2, 3, 4, 5, 6, 7] and even animals [8, 9, 10]. Such work splits the system’s configuration space into a position space and an internal shape space. These efforts then describe analytic tools, using constructs such as *connection vector fields* and *constraint curvature functions* [11], to compute

a path in the shape space that induces a desired displacement in the position space. Typically these shape space paths are cyclic, and thus are termed *gaits*. Past work with geometric mechanics views the shape space using charts in a Euclidean space; for example, when the shape space has two dimensions, its parameterization is in \mathbb{R}^2 . This paper considers systems whose internal degrees of freedom are cyclic and therefore Euclidean parameterizations do not capture the true essence of the shape space.

This paper considers shape spaces that are tori or cylinders. Consider the yellow gait in Fig. 1; it is a cycle in the parameterization. However, the green gait appears to be a non-closed curve in its parameterization, thereby preventing us from using previously derived gait-design tools.

Additionally, the non simply-connected topology of the true shape space raises another subtle problem. Recall that a vector field can be decomposed via the Hodge-Helmholtz decomposition [12, 13] into two component vector fields: a curl-free component and a divergence-free component. When integrating a closed loop in a puncture-free Euclidean space (or Euclidean parameterization), the curl-free contribution is identically zero because the curl-free field is conservative in a simply connected space [12]. However, the curl-free field is not conservative on non-simply connected spaces, such as a torus, and therefore may have a non-zero contribution for gaits that wrap around the cyclic dimensions of the space space.

The contribution of this paper is to develop the calculus to account for the curl-free contribution of the gait on toroidal and

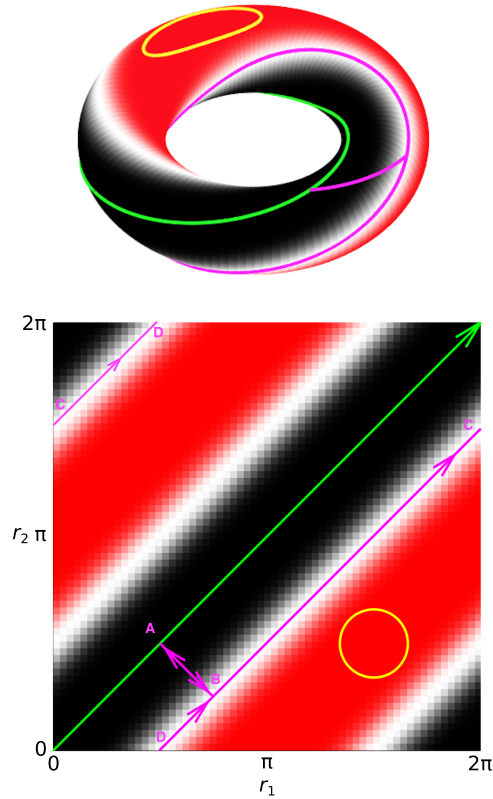


FIGURE 1. Constraint curvature function for a differential drive car plotted on a torus shape space and its Euclidean parameterization. The yellow circle is a gait that does not wind around the torus and the green line a gait that winds around both cyclic components of the shape space. The pink curve is a gait for parallel parking maneuver discussed later in this paper. Red regions are positive (out of the page) and black regions are negative (into the page). The torus has been “cut” along both of its cyclical dimensions, so that both points labelled D coincide on the torus, as do both points labelled C . The pink curve is, on the torus, a single closed curve. The scaling of the heights and width between stripes depends on the dimensions chosen for the car.

cylindrical shape spaces and thereby extend the analysis and design of gaits that wind through cyclical dimensions of the shape space. In doing so, this paper extends the applicability of the gait design, analysis, and visualization tools that use connection vector fields and constraint curvature functions to a larger set of motions. As an example, using these tools, we can now provide a differential geometric rationale to common gaits for the differential drive car. Additionally, this paper takes a new view at analyzing snake robots: previous related work used sinusoids as basis functions in a shape space. With the tools derived in this paper, we can design gaits in a shape space parameterized directly by amplitude and phase, which makes gait design easier. Finally, we apply the results of this paper to legged systems,

where we parameterize motions in terms of phase variables rather than directly on joint angles. These methods allow us to plan for systems with higher dimensional shape spaces, if some variables can be linked together by underlying phase variables on \mathbb{S}^1 , such as a footfall pattern for a legged system.

2 BACKGROUND

Geometric mechanics is a discipline that builds on differential geometry and classical mechanics [1]. Geometric mechanics leverages the symmetric properties of the locomotion system. When the system’s inertia can be neglected, the equation of motion is simplified to the following form (known as the *kinematic reconstruction equation*),

$$\xi = -A(r)\dot{r} \quad (1)$$

where ξ is the body velocity, r is the system shape variables (either the joint angles or a function of the joint angles) in the shape space M , and $A(r)$ is called *the local connection*, a matrix that maps changes in shape to body velocities. In these systems, no additional momentum can be built, so the body stops moving immediately when the joints stop moving. Note that $A(r)$ is a function of shape r and each row of $A(r)$ represents a vector field defined over the shape space. This vector field is called the *connection vector field* [11].

Prior work used the tools of geometric mechanics to find gaits to move or turn the system in a desirable direction [1, 11, 3, 5, 6, 14]. The displacement of the system $\zeta(T)$ as a result of executing a gait Φ is therefore computed as the line integral of the connection vector field along the gait,

$$\zeta(T) = \int_{\Phi} A(r) dr. \quad (2)$$

where T is the period of the gait. Assuming a Euclidean parameterization of a two-dimensional shape space, for instance if joints have finite limits, one can further apply Green’s form of Stokes’s theorem to convert this line integral into an area integral,

$$\zeta(T) = \iint_{\Omega} \text{curl} A(r) dr_1 dr_2 \quad (3)$$

where Ω is the area enclosed by the gait. Now, the displacement of a gait can be determined by integrating the curl of the connection over an area enclosed by the gait. Likewise, one can plot the curl of the connection vector field, and then by inspection prescribe gaits [3], or optimize gaits for displacement or power per cycle [5, 6]. The curl of the connection vector field is called the constraint curvature function [11].

Since we are considering gaits that winds around the \mathbb{S}^1 component of the shape space, we need to establish terminology that measures the number of winds. Conventionally, a winding number is defined by the number of revolutions a closed loop curve makes in the plane [15]. With slight abuse of notation, we define the winding number, $w \in \mathbb{Z}^m$ for an m -dimensional space to be the integer set of times that a path wraps around each \mathbb{S}^1 dimension of that space. This notion of winding number is similar to that which is defined in [16]. For gaits that have a zero winding number, the use of the curvature visualization tool is straightforward, as described in [2]. However, gaits with non-zero winding numbers do not have a closed curve representation on the parameterization of the shape space, so do not enclose a well defined area. Consequently, the curvature-visualization tools cannot be used for such gaits.

Moreover, recall the Hodge-Helmholtz decomposition separates a vector field into a curl-free component and a divergence-free component. In a simply connected shape space, the curl-free component forms a conservative vector field, and sometimes is referred to as the conservative contribution. When the gait in a simply-connected shape space is a closed curve, the the path integral along the curl-free part of vector field does not contribute to the line integral because the line integral along a closed path in a conservative vector field is zero. In such a case, only the divergence-free part of the original vector field needs to be considered when taking the line integral. This observation will prove useful when deriving our contribution in this paper.

3 CONSTRAINT CURVATURE FUNCTIONS IN TORUS SHAPE SPACES

Although successfully applied to a variety of systems, prior work [11, 4, 2] treated the shape space as simply connected and Euclidean. Assuming that the shape space is simply-connected, the curl-free portion of the connection vector field is conservative, and therefore has no contribution to the total displacement. In this section, we show how to explicitly account for both the curl-free and divergence-free portions of the connection vector field on a non-simply connected shape space, i.e., the torus. With the curl-free and divergence-free contributions in-hand, we demonstrate how to effectively combine them and subsequently use this to prescribe gaits on a torus.

Consider the connection vector field of a system with a toroidal shape space, $\mathbb{T}^2 = \mathbb{S}^1 \times \mathbb{S}^1$. First, we plot the vector field under a chart to a subset of \mathbb{R}^2 , such that every point on the torus is represented by exactly one point on the chart, except at the open boundary of the parameterization. This chart “unwraps” the torus. We can see now that closed gaits on the torus may not appear as closed on the chart, and could have a variety of winding numbers. See Fig. 2 for illustrative examples of paths with different winding numbers on the unwrapped torus shape space.

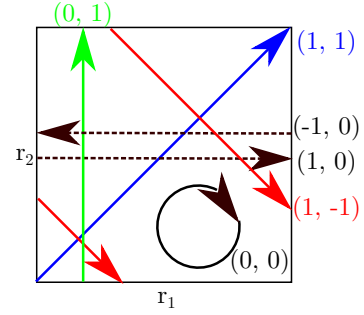


FIGURE 2. Various possible shape space winding numbers on a toroidal shape space, with shape parameters r_1 and r_2 . This is a chart on a torus, the top and bottom boundaries are equivalent, and the left and right boundaries are equivalent. Multiple winds around the torus are possible, and would have larger integer winding numbers.

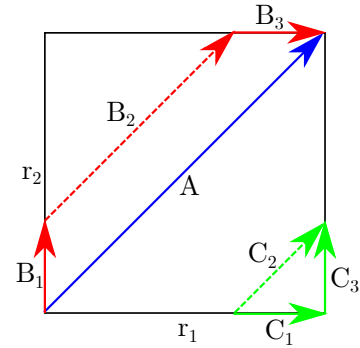


FIGURE 3. Illustration for Lemma III.1

3.1 Curl-free Contribution of Connection Vector Fields

Lemma 3.1. In the curl-free component of the connection vector field, gaits with the same winding number have the same line integral, independent from the starting points and the trajectories of the gaits.

Proof: Consider a chart of the curl-free component of the connection vector field in a toroidal shape space, as shown in Fig. 3. First, we take two gaits A and B; B is composed of three segments B_1 , B_2 and B_3 , and both gaits connect the bottom left and top right corners of the shape space i.e. $(0,0)$ to $(2\pi, 2\pi)$. The shape space is parameterized by vector $r \in \mathbb{S}^1 \times \mathbb{S}^1$. These paths appear open on the chart, but on the torus, the left and right sides of this chart are connected, and the top and bottom of the chart are connected. We know that in a conservative vector field, the line integral along a closed loop is zero.

$$-\int_A A(r)dr + \int_{B_1} A(r)dr + \int_{B_2} A(r)dr + \int_{B_3} A(r)dr = 0$$

upper left panel of Fig. 4. This curve is drawn on a chart of the torus where the left and right boundaries, and the bottom and top boundaries are respectively identified with each other. The curve P is not closed in the chart but is indeed closed on the torus. We next close the loop on the chart by drawing a path along the boundaries of the chart (the green paths G in Fig. 4). To account for the extra displacement that will be generated by integrating along the added paths, we use the superposition principle and add equal and opposite paths (the red paths R in Fig. 4).

3.3 Contributions from both Curl-free and Divergence-free Vector fields

The path integral of the vector field along the gait is the sum of the following components: two from the curl-free part of the vector fields and two from the divergence-free part of the vector fields, i.e.,

- i A closed loop in the curl-free field, which evaluates to zero (Fig. 4(1), $P_C + G_{C1} + G_{C2}$)
- ii A set of paths travelling the same winding number as the gait, in the curl-free field. (Fig. 4(2), $R_{C1} + R_{C2}$)
- iii A closed loop in the divergence-free field, which includes the gait and a path traversing the chart boundary. (Fig. 4(3), $P_{NC} + G_{NC1} + G_{NC2}$)
- iv A set of paths travelling the same winding number as the gait, in the divergence-free field. (Fig. 4(4), $R_{NC1} + R_{NC2}$)

The first component (i) is zero and the third component (iii) can be determined using constraint curvature functions, as described in Sec. 2. Note that the second (ii) and fourth (iv) components are the same path. The contribution from the second and fourth components can be determined by simply computing the path integral of this path in both the curl-free and divergence-free fields, and then summing the two results. Or, we can compute the path integral of this path in the original vector field. Finally, the full body velocity integral is the sum of these components.

We remark that for gaits with non-zero winding numbers, it is not important whether the integral is taken above/below or to the left/right of the gait path. To show this, consider the paths around the four sides of a chart on a toroidal shape space, as shown in Fig. 5. The paths P_1 , P_2 , P_3 , and P_4 form a closed loop. Yet, the left and right sides are the same path on the torus, $\int_{P_1} A(r)dr = -\int_{P_3} A(r)dr$ and similarly, $\int_{P_2} A(r)dr = -\int_{P_4} A(r)dr$. As a result, the total path integral is zero, and so by Stokes' theorem, the area integral of the path around the chart boundary is zero. Further, for a gait with a non-zero winding number that divides the space, the area integrals on the two sides of the gait must sum to zero. Consider for example the gait $G_{(1,1)}$ that belongs to $(1,1)$ winding number family. The integral of curl of the connection vector field over the area enclosed below

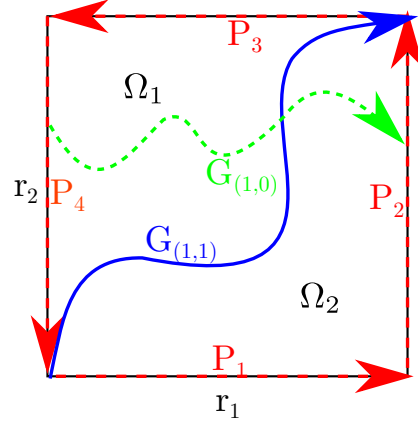


FIGURE 5. Paths drawn on a chart of a toroidal shape space. The paths P form a closed loop, but since the sides of the torus are connected on the underlying manifold, $\int_{P_1} = -\int_{P_3}$ and $\int_{P_2} = -\int_{P_4}$. The total path integral of P is zero, and so the area integral of P is zero. Further, for gaits with non-zero winding numbers like $G_{(1,1)}$ and $G_{(1,0)}$, the area integrals above and below will be the same magnitude but opposite sign, as they must sum to zero.

the gait is

$$\begin{aligned}
 I_{below} &= \iint_{\Omega_2} \text{curl } A(r) dr_1 dr_2 \\
 &= \int_{P_1} A(r)dr + \int_{P_2} A(r)dr - \int_{G_{(1,1)}} A(r)dr \quad (5)
 \end{aligned}$$

Likewise, the integral of curl of the connection vector field over the area enclosed above the gait is

$$\begin{aligned}
 I_{above} &= \iint_{\Omega_1} \text{curl } A(r) dr_1 dr_2 \\
 &= \int_{P_4} A(r)dr + \int_{G_{(1,1)}} A(r)dr + \int_{P_3} A(r)dr \quad (6)
 \end{aligned}$$

Summing up Eq. 6 and Eq. 5 gives:

$$\begin{aligned}
 I_{total} &= I_{below} + I_{above} \\
 &= \int_{P_1} A(r)dr + \int_{P_2} A(r)dr - \int_{G_{(1,1)}} A(r)dr \\
 &\quad + \int_{P_4} A(r)dr + \int_{G_{(1,1)}} A(r)dr + \int_{P_3} A(r)dr \\
 &= \int_{P_1} A(r)dr + \int_{P_3} A(r)dr \\
 &\quad + \int_{P_2} A(r)dr + \int_{P_4} A(r)dr \\
 &= 0 \quad (7)
 \end{aligned}$$

$$\begin{aligned} \Rightarrow \iint_{\Omega_1} \text{curl } A(r) dr_1 dr_2 + \iint_{\Omega_2} \text{curl } A(r) dr_1 dr_2 &= 0 \\ \Rightarrow \iint_{\Omega_1} \text{curl } A(r) dr_1 dr_2 &= - \iint_{\Omega_2} \text{curl } A(r) dr_1 dr_2 \quad (8) \end{aligned}$$

3.4 Gait planning steps

To design a gait for a system with a torus or cylindrical shape space, we have developed the following procedure:

- Compute the connection of the system and the connection vector field, either analytically [4] or empirically [3]. Select a chart that covers the space once, e.g., where each cyclical shape variable is plotted on $(-\pi, \pi)$.
- Compute the path integral along one cycle of each cyclical shape variable. For convenience, we use the bottom of the chart such as the path R_1 and right of the chart such as R_2 . This path integral in the full vector field, is the sum of the curl-free (item ii in Sec. 3.3) and divergence-free components (item iv). Note the sign of each line integral, as this will influence the choice of gait.
- Plot the curl of the connection vector field as a constraint curvature function.
- Choose a gait that maximizes the positive or negative area enclosed by the gait path and the boundary of the chart. We choose the gait winding number and path to maximize positive or negative area based on the chart boundary line integral from step (b).
- Sum the contributions from the boundary line integrals, multiplied by their winding numbers, with the constraint curvature function area integral.

For example, if the boundary line integral for r_1 is L_1 where ($L_1 > 0$), and for r_2 is negative, ($L_2 < 0$) we may choose a gait with a winding number $w = (1, -1)$ then look for gaits that enclose a positive area. The resulting gait would have a body velocity integral (an approximation of the net displacement) characterized by

$$\zeta(T) = \int_{\Phi} A(r) dr = w_1 L_1 + w_2 L_2 + \iint_{\Omega} \text{curl}(A(r)) dr_1 dr_2$$

where Ω is the area enclosed by the gait Φ . This method can be applied to cylindrical shape spaces in which only one shape parameter is cyclical. In these cases, the winding number of non-cyclical shape parameters must be zero, but otherwise the above method remains unchanged. Similarly, gaits can still be designed on torus or cylinder shape spaces with winding number zero for all shape parameters, in which case this method produces the same results as in prior work.

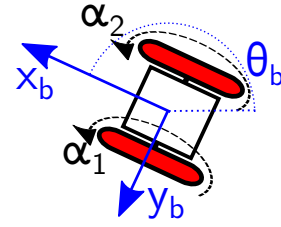


FIGURE 6. Differential drive car model.

4 DIFFERENTIAL DRIVE CAR EXAMPLE

4.1 Model and Method

The kinematic differential drive car's model has been studied in past geometric analysis. This model has shape variables r_1, r_2 , the rotation angles of the left and right wheels of the car.

In [11], the differential drive car was analyzed in the south pointing chariot frame, a frame that counter-rotates with respect to body frame by an angle $\theta = r_1 - r_2$. In this frame, the local connection for ξ_θ is nullified and thus makes the constraint curvature function integration in x or y axes in body frame equivalent to the displacement in world frame. Assuming the width of the car to be 1 unit and the radius of the wheel to be 2 units, the resulting local connection is given by:

$$\xi = \begin{bmatrix} \cos(r_1 - r_2) & \cos(r_1 - r_2) \\ \sin(r_1 - r_2) & \sin(r_1 - r_2) \\ 0 & 0 \end{bmatrix} \dot{r}. \quad (9)$$

To analyze and design gaits, we first compute the constraint curvature function of the system by using Stokes' Theorem based on the local connection Eq. 9. In Fig. 1, we visualize the computed constraint curvature function for displacement along y axis.

The most obvious gait for a differential drive car is both wheels rolling forward as this leverages the full range of the joint and produces maximal displacement per joint revolution. Such a gait would be represented by a straight path through the shape space like the green path in Fig. 1.

4.2 Gait Design on Torus

Our objective in gait design is to determine the sequence of periodic wheel rotations that generate maximum displacement per cycle. This is nothing but the sum of two components: (1) The curl of the connection vector field over an area enclosed by a curve (yet to be determined) and the chart boundaries, and (2) the line integral of the connection vector field along the chart boundary.

For example, the goal for a parallel parking gait is to find a curve on the constraint curvature function that enclose the maximum area integral in the x_b direction. In Fig. 1, the red and the

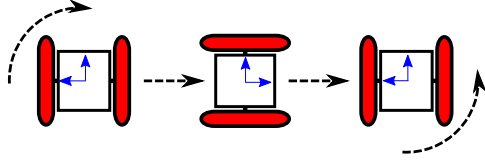


FIGURE 7. Differential drive car executing a parallel parking gait

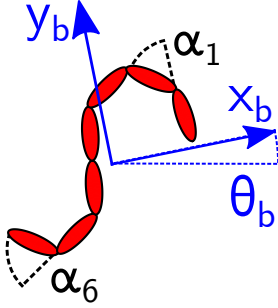


FIGURE 8. The snake-like swimmer model used in Sec. 5.1. This planar model swims in a viscous fluid. As a body frame, we choose the “average” body frame, taken from the average joint angles and average link locations.

black area correspond to opposite signs of the constraint curvature function’s value. By adding lines along the boundary of the chart and using the method mentioned in previous sections (3.4), the pink curve, which traverses configurations “A”, “B”, “C”, “D”, “B”, “A” in sequence, is the result obtained that maximizes the enclosed area integral, and the displacement in y direction is 4π .

If we visualize the motion of the car along this curve in Fig 7, it is an intuitive optimal gait for parallel parking by turning the car by 90° , going straight and then counter-turning 90° . This gait has a winding number of (1,1).

5 SNAKE-LIKE SWIMMER EXAMPLE

5.1 Model and Method

The N -link planar low Reynolds number swimmer has served a fertile prototype for geometric gait design. The total configuration space Q of the planar swimmer can be split into a position space G and an internal shape space M , i.e., $Q = G \times M$ [17]. Any element $g \in G$, where in our case $G = SE(2)$, represents the position and orientation of the body frame of a reference link on the swimmer with respect to the world frame. The internal shape space $M = \prod_{i=1}^{N-1} (\mathbb{S}^1)$ is characterized by angles $(\alpha_1, \dots, \alpha_{N-1})$. With this natural splitting, we can derive the kinematic reconstruction equation (10), that relates changes in the internal shape of the swimmer to its motion in the inertial frame. A detailed derivation of the equations of motion for this

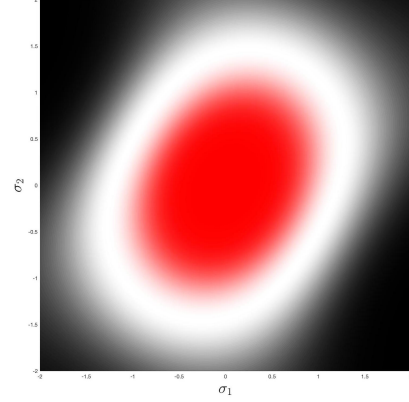


FIGURE 9. The connection curvature function in the the x_b (forward) direction for a seven-link swimmer. This function is created from the serpenoid equation parameterization in Eq. 11

system can be found in [4],

$$\xi = -A(\alpha)\dot{\alpha} \quad (10)$$

where $A(\alpha) \in \mathbb{R}^{3 \times N-1}$ is known as the local form of a connection. It maps shape velocities to body velocities: $A(\alpha) : \prod_i T_{\alpha_i} \mathbb{S}^1 \rightarrow \mathfrak{se}(2)$. Eq. (10) is known as the *kinematic reconstruction equation*.

To coordinate the many joints using a smaller number of parameters, a shape basis function called the *serpenoid curve* [18] is employed, prescribing the angle α_i of each joint $i \in \{1, 2, \dots, N-1\}$ in the swimmer as

$$\alpha_i = \sigma_1 \sin(\Omega i) + \sigma_2 \cos(\Omega i) \quad (11)$$

where Ω is the spatial frequency of the curve, and the weights σ are shape parameters that describe the sine and cosine components of the curve. When the weights σ are varied cyclically, a travelling wave gait can be created and the system swims forward. For instance, a gait with a constant amplitude is represented as a circle in this shape space. In past works using constraint curvature functions, gaits are formed from a cycle in the w shape space, that is, with $r = [\sigma_1, \sigma_2]^T$. The local connection $A(r)$ can be rewritten in terms of the new shape parameters [4]. But, a gait with two shape variables can also be parameterized by a reciprocating phase and an amplitude [19]. For the serpenoid swimmer, we can therefore reparameterize the gait Eq. (11) as a travelling wave with variable amplitude,

$$\alpha_i = \mathcal{A} \cos(\Omega i - \phi) \quad (12)$$

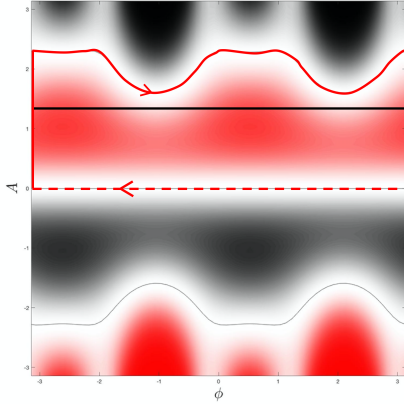


FIGURE 10. The connection curvature function, on an unwrapped cylinder, in the the x_b (forward) direction for a seven-link swimmer. This function is created from the serpenoid equation parameterization in Eq. 12. The paths drawn onto this plot represent gaits described in Sec. 5.2

with amplitude $\mathcal{A} = \sqrt{(\sigma_1^2 + \sigma_2^2)}$ and phase $\phi = \tan^{-1}(\sigma_2/\sigma_1)$. In this form, the shape space is $r = [\phi, \mathcal{A}]^T$. The phase can be viewed as cyclical; $\alpha_i(0, \mathcal{A}) = \alpha_i(2\pi, \mathcal{A})$ so we can consider $\phi \in \mathbb{S}^1$. Fig. 10 depicts the constraint curvature functions of the swimmer represented on the cylindrical parameterization of the shape space. We used $\Omega = \frac{2\pi}{N-1}$, $N = 7$ links, for these simulations.

5.2 Gait design on a cylinder

In this shape space, we can construct gaits with large body velocity integrals. To facilitate gait design, we can now assume that the phase variable ϕ increases constantly in time as this generates a traveling wave along the swimmer's backbone. The search for a gait in this space is thus reduced to selecting a cyclical amplitude, a path from one side of the chart to the other, which encloses a net area below the curve. The simplest way to select this curve is to chose a constant amplitude represented as the solid black line in Fig. 10. However, gaits with larger displacements can be found by allowing a variable amplitude. We can use the procedure described in Sec 3.4, along with numerical optimization (such as that described by [5]) to design a profile for amplitude that produces more displacement. Out of the shape parameters \mathcal{A} and ϕ , only \mathcal{A} needs to be chosen as a function of time. Representing the curvature as a function of \mathcal{A} and ϕ , allows us to pick a region and its boundary on the height function plot that can serve as an initial seed in a numerical optimizer. One such curve is the red curve shown in Fig 10.

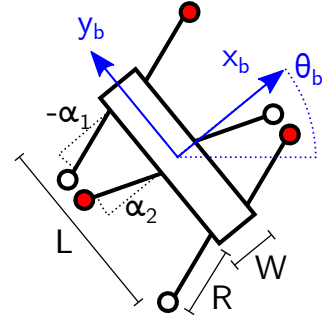


FIGURE 11. Hexapod model. Each leg has two degrees of freedom: a joint at its base, and a raise/lowering of the foot. Red areas represent full contact with the ground, and white represents no contact. The legs are coordinated in an alternating tripod gait. We used body length $L = 1$, width $W = 0.3$, and leg length $R = 0.3$.

6 HEXAPOD EXAMPLE

Many locomoting systems, such as walking robots, rely on making and breaking contacts with the ground. While related previous work [9] presented a method to include contact states into a geometric mechanics model, there has not been a method to encode those contacts within a constraint curvature function. Here we introduce a method to include the *footfall pattern*, the contact pattern describing the stance or flight phases of the feet in the shape basis parameterization and the constraint curvature function. This allows us to plan gaits for a given footfall pattern, and investigate the limb coordination needed for effective locomotion.

We introduce a simple hexapod model, where each leg i has a single hip joint with angle α_i and foot contact value C_i . We restrict the legs to an alternating tripod gait, common in both hexapedal arthropods [20] and robots [21, 22]. To form an alternating tripod gait, we link the joint angles for legs 1, 3, 5 to those of legs 2, 4, 6. The corresponding linear shape basis functions would be:

$$\begin{aligned} \beta_1 &= [0, 1, 0, 1, 0, 1]^T \\ \beta_2 &= [1, 0, 1, 0, 1, 0]^T \\ \alpha &= \beta_1 \kappa_1 + \beta_2 \kappa_2 \end{aligned} \quad (13)$$

where the shape basis parameters correspond to the tripod angles, $r = [\kappa_1, \kappa_2]^T$, $w \in \mathbb{R}^2$. We model the system locomoting through an overdamped viscous media, where the equations of motion are derived in the same manner as described in Sec. 5.1. This would correspond to feet moving through viscous or granular media like sand or mud, where the feet take a finite time to extract or place in the media. While a more realistic model would be a resistive force theory model for granular media [2, 10] could be applied, we choose a linear drag law in this example for simplicity.

In order for a contact pattern to be included in the local connection, it must be parameterized in terms of only the shape parameters r and may not include their derivatives, so that the equations of motion can be written in the form of 1. However, we observe that with the shape basis parameterization in Eq. 13, it is not possible to create a contact pattern function solely in terms of the shape parameters and use methods presented by prior work. For instance, the gait would need to pass through the point $r = [0, 0]$ twice per cycle, with different contact states depending on whether the foot is moving forward or backward.

To analyze an alternating tripod gait with constraint curvature functions, we can reparameterize the shape space using cyclical phase variables, $\phi \in \mathbb{T}^2$, where the tripods are coordinated with shape basis functions,

$$\begin{aligned}\beta_{\phi_1} &= [1, 0, 1, 0, 1, 0]^T \sin(\phi_1) \\ \beta_{\phi_2} &= [0, -1, 0, -1, 0, -1]^T \sin(\phi_2) \\ \alpha &= \beta_{\phi_1} + \beta_{\phi_2}\end{aligned}\quad (14)$$

in which each shape bases β_ϕ are a nonlinear function of shape parameters ϕ . The foot contact function can then be expressed

$$C_i = \begin{cases} 0 & 0 \leq \phi_i < \frac{\pi}{2}, \frac{3\pi}{2} \leq \phi_i < 2\pi \\ 1 & \frac{\pi}{2} \leq \phi_i < \frac{3\pi}{2} \end{cases} \quad (15)$$

where C_i is the contact state of tripod $i \in \{1, 2\}$.

By creating a contact function in terms of shape variables, we allow the footfall pattern to be implicitly encoded in the constraint curvature function for any gaits created in terms of the shape basis parameters. The connection can be expressed in terms of the new shape parameters $r = [\phi_1, \phi_2]^T$, and the constraint curvature functions drawn. We are now able to plan a gait wrapping around the toroidal shape space. The constraint curvature function and a gait are shown in Fig. 12.

The model used in this example does not correspond precisely to any realistic animal or robot, but instead illustrates the process of gait planning on non-euclidean shape spaces by reparameterizing the shape with phase variables. This allows us to include additional degrees of freedom, synchronized to the two primary shape variables via footfall patterns, and still visualize or optimize the gait efficacy with constraint curvature functions.

7 DISCUSSION

We have shown how constraint curvature function-based gait analysis can be applied to cylindrical or toroidal shape spaces. As a consequence, we are able to analyze a broader class of systems and gaits by parameterizing the coordination among multiple degrees of freedom with cyclical phase variables. While we chose to explore this new method on three example systems, there are

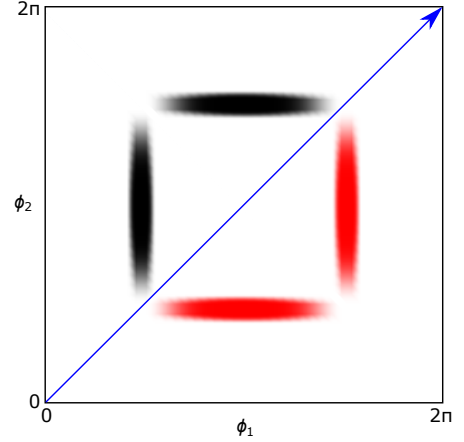


FIGURE 12. The hexapod constraint curvature function for forward locomotion, with one possible gait drawn as a path in blue. The underlying shape space for this parameterization is a torus. The feet interact with the environment through a linear isotropic drag with viscous drag constant of 100 in both the translation and rotation directions.

many others to which this work is applicable, such as the Purcell three link swimmer parameterized by amplitude and phase as in [19], or a kinematic Ackerman car.

In some sense, since all gaits are cyclical, it is possible to write some parameterization of shape variables in terms of some combinations of amplitudes and phases for *any* system, and for those with many possible contact states, for any contact pattern. Such a reparameterization, followed by constructing a constraint curvature function, means that gaits formerly forming close loops on Euclidean spaces can be “unrolled” under a change to non-euclidean variables. One consequence of this unrolling is that gait construction could now be conducted in what is effectively a lower dimensional space, with the assumption that the phase variables are constantly increasing. For example, related past work [3, 4] constructed gaits for snake-like swimmers by choosing points in the Euclidean shape space that form a closed loop. By reparameterizing to a cylindrical shape space, the gait design problem can be posed as finding a path across the shape space that starts and ends at the same amplitude, and choosing one amplitude value for each point in the phase.

8 CONCLUSION

The three systems we have analyzed in this paper are meant to exemplify the range of systems to which our methods are applicable. In future work we will apply these ideas to study other robotic and biological models. For instance, many animals locomote through sand and mud, on flat and sloped surfaces. Past related work revealed that limb-tail coordination is necessary for effective locomotion, especially on sloped surfaces [10]. With our new tools, we can study salamander and lizard locomotion

with various footfall patterns and on sloped granular media [23].

We will continue to improve constraint curvature function-based gait optimization for systems with cyclical phase variables. In systems with high-dimensional shape spaces, our method could help investigate optimal coordination strategies and footfall patterns, potentially using tools like shape-basis [4] or geometric gait optimization [6]. We will investigate the application of these methods to systems with continuous rotation components. For instance, we can now analyze Purcells' three link swimmer with no joint limits, or systems with propellers alongside fins and an actuated spine, to create new types of robots swimming at low Reynolds numbers. Our results also reveal another insight: *the topological structure of the shape space is a result of the parameterization chosen, and is not necessarily a property of the system*. In future work we hope to discover rules about which shape space topologies apply to a given system, and to explore how geometric methods can be applied to any shape space topology.

REFERENCES

- [1] Kelly, S. D., and Murray, R. M., 1995. "Geometric phases and robotic locomotion". *Journal of Field Robotics*, **12**(6), pp. 417–431.
- [2] Hatton, R. L., Ding, Y., Choset, H., and Goldman, D. I., 2013. "Geometric visualization of self-propulsion in a complex medium". *Physical review letters*, **110**(7), p. 078101.
- [3] Dai, J., Faraji, H., Gong, C., Hatton, R. L., Goldman, D. I., and Choset, H., 2016. "Geometric Swimming on a Granular Surface.". In *Robotics: Science and Systems*.
- [4] Gong, C., Goldman, D. I., and Choset, H., 2016. "Simplifying Gait Design via Shape Basis Optimization.". In *Robotics: Science and Systems*.
- [5] Ramasamy, S., and Hatton, R. L., 2016. "Soap-bubble optimization of gaits". In *Decision and Control (CDC), 2016 IEEE 55th Conference on*, IEEE, pp. 1056–1062.
- [6] Ramasamy, S., and Hatton, R. L., 2017. "Geometric gait optimization beyond two dimensions". In *American Control Conference (ACC), 2017*, IEEE, pp. 642–648.
- [7] Melli, J. B., Rowley, C. W., and Rufat, D. S., 2006. "Motion planning for an articulated body in a perfect planar fluid". *SIAM Journal on applied dynamical systems*, **5**(4), pp. 650–669.
- [8] Aguilar, J., Zhang, T., Qian, F., Kingsbury, M., McInroe, B., Mazouchova, N., Li, C., Maladen, R., Gong, C., Travers, M., Hatton, R. L., Choset, H., Umbanhowar, P. B., and Goldman, D. I., 2016. "A review on locomotion robophysics: the study of movement at the intersection of robotics, soft matter and dynamical systems". *Reports on Progress in Physics*, **79**(11), p. 110001.
- [9] Gong, C., Travers, M., Astley, H. C., Goldman, D. I., and Choset, H., 2015. "Limbless locomotors that turn in place". In *International Conference on Robotics and Automation (ICRA)*, IEEE, pp. 3747–3754.
- [10] McInroe, B., Astley, H. C., Gong, C., Kawano, S. M., Schiebel, P. E., Rieser, J. M., Choset, H., Blob, R. W., and Goldman, D. I., 2016. "Tail use improves performance on soft substrates in models of early vertebrate land locomotors". *Science*, **353**(6295), pp. 154–158.
- [11] Hatton, R. L., and Choset, H., 2011. "Geometric motion planning: The local connection, Stokes theorem, and the importance of coordinate choice". *The International Journal of Robotics Research*, **30**(8), pp. 988–1014.
- [12] Hatton, R. L., and Choset, H., 2015. "Nonconservativity and noncommutativity in locomotion". *European Physical Journal Special Topics*, **224**(17-18), pp. 3141–3174.
- [13] Bhatia, H., Norgard, G., Pascucci, V., and Bremer, P.-T., 2013. "The helmholtz-hodge decomposition survey". *IEEE Transactions on visualization and computer graphics*, **19**(8), pp. 1386–1404.
- [14] Burton, L., Hatton, R., Choset, H., and Hosoi, A., 2010. "Breaking Symmetry with Gravity: Two-Link Swimming Using Buoyant Orientation". In *APS Division of Fluid Dynamics Meeting Abstracts*.
- [15] Millman, R. S., and Parker, G. D., 1977. *Elements of differential geometry*. Prentice Hall.
- [16] McIntyre, M., and Cairns, G., 1993. "A new formula for winding number". *Geometriae Dedicata*, **46**(2), pp. 149–159.
- [17] Ostrowski, J., and Burdick, J., 1998. "The geometric mechanics of undulatory robotic locomotion". *The international journal of robotics research*, **17**(7), pp. 683–701.
- [18] Hirose, S., Cave, P., and Goulden, C., 1993. *Biologically inspired robots: serpentine locomotors and manipulators*. Oxford University Press.
- [19] Wiezel, O., and Or, Y., 2016. "Using optimal control to obtain maximum displacement gait for Purcell's three-link swimmer". In *2016 Conference on Decision and Control*, IEEE, pp. 4463–4468.
- [20] Wöhrle, T., Reinhardt, L., and Blickhan, R., 2017. "Propulsion in hexapod locomotion: how do desert ants traverse slopes?". *Journal of Experimental Biology*, **220**(9), pp. 1618–1625.
- [21] Saranli, U., Buehler, M., and Koditschek, D. E., 2001. "Rhex: A simple and highly mobile hexapod robot". *The International Journal of Robotics Research*, **20**(7), pp. 616–631.
- [22] Travers, M., Ansari, A., and Choset, H., 2016. "A dynamical systems approach to obstacle navigation for a series-elastic hexapod robot". In *Decision and Control (CDC), 2016 IEEE 55th Conference on*, IEEE, pp. 5152–5157.
- [23] Zhong, B., et al., 2018. "Coordination of back bending and leg movements for quadrupedal locomotion". In *Robotics: Science and Systems*.